Society For Biomaterials

A foldable manipulator with tunable stiffness based on braided structure

Zufeng Shang,[1,2] **Jiayao Ma**,[1,2] **Zhong You**,[2,3] **Shuxin Wang**[1,2]

[1]Key Laboratory of Mechanism Theory and Equipment Design of Ministry of Education, Tianjin University, 135 Yaguan Road, Tianjin 300350, China
[2]School of Mechanical Engineering, Tianjin University, 135 Yaguan Road, Tianjin 300350, China
[3]Department of Engineering Science, University of Oxford, Parks Road, Oxford, OX1 3PJ, UK

Received 7 December 2018; revised 12 March 2019; accepted 4 April 2019
Published online 00 Month 2019 in Wiley Online Library (wileyonlinelibrary.com). DOI: 10.1002/jbm.b.34390

Abstract: Minimally invasive surgery (MIS) has recently seen a surge in clinical applications due to its potential benefits over open surgery. In MIS, a long manipulator is placed through a tortuous human orifice to create a channel for surgical tools and provide support when they are operated. Currently the relative large profile and low stiffness of the manipulators limit the effectiveness and accuracy of MIS. Here we propose a new foldable manipulator with tunable stiffness. The manipulator takes a braided skeleton to enable radial folding, whereas membrane is used to seal the skeleton so as to adjust stiffness through creating negative pressure. We demonstrated experimentally, numerically, and analytically that, a flexible and a rigid state were obtained, and the ratio of bending stiffness in the rigid state to that in the flexible state reached 6.85. In addition, the manipulator achieved a radial folding ratio of 1.95. The proposed manipulator shows great potential in the design of surgical robots for MIS. © 2019 Wiley Periodicals, Inc. J Biomed Mater Res Part B: 00B: 000–000, 2019.

Key Words: minimally invasive surgery, braided structure, tunable stiffness, folding ratio

How to cite this article: Shang Z, Ma J, You Z, Wang S. 2019. A foldable manipulator with tunable stiffness based on braided structure. J Biomed Mater Res Part B. 2019:00B:1–10.

INTRODUCTION

Minimally invasive surgery (MIS) has been rapidly adopted in a wide range of clinical applications[1–4] due to its advantages over conventional open surgery, including smaller scars, less postoperative pain, shorter hospitalization, and earlier rehabilitation.[5–7] As a newly developed type of MIS, natural orifice transluminal endoscopic surgery (NOTES) accesses lesion via transoral, transcolonic, or transvaginal routes, thereby further reducing tissue damage and recovery time.[8,9]

During NOTES, a long snake-like manipulator is first inserted through a natural body orifice. When it reaches the lesion, miniaturized surgical tools pass through the manipulator and perform operations.[10] During insertion, the manipulator is required to be compact in size[11] and flexible[12] so as to go through the torturous cavity without kinking or damaging the inner wall of the cavity.[13,14] During operation, on the other hand, the manipulator needs to be large to provide more space for surgical tools and rigid to support them.[11,12] As a result, there exist two pairs of conflicts, stiffness, and size. Developments of surgical instruments to fulfill those conflicting requirements are essential for the wide applications of NOTES. Conventional rigid surgical tools and flexible endoscopes can only partially satisfy the requirements and are therefore not directly applicable in NOTES.[15,16]

To tackle the conflict of stiffness, snake-like manipulators with stiffening mechanism have also been extensively studied. One method to change stiffness is to increase the friction between rigid links by amplifying the control wire tension.[13] Nevertheless, high stiffness requires high wire tension, and the links need to be large enough to sustain the load, making it difficult to create a compact manipulator. Phase-change materials which can transform between liquid and solid states with temperature change[16–19] and thermoplastic polymers whose elasticity modulus is tunable by temperature,[20,21] have also been applied to design locking mechanisms. A wide range of stiffness can be obtained with this method, but long activation timescale limits its application in practice. Pneumatic or hydraulic shape-locking mechanism, which functions by compressing discrete parts together with controllable fluid pressure,[22–25] shows great promise. With friction or geometric locking, the stiffness can be tunable almost instantaneously. Despite the efforts, the other pair of conflict, that is, size, is rarely explored.

Foldable structures, a special kind of structures, which are able to dramatically change their configurations so as to change sizes,[26] could provide a solution to this problem. Especially, the braided tube, made of fibers interwoven in a crisscross pattern to form a tubular mesh configuration,[27] can significantly reduce its diameter when longitudinally

Correspondence to: J. Ma; e-mail: jiayao.ma@tju.edu.cn and S. Wang; e-mail: shuxinw@tju.edu.cn
Contract grant sponsor: National Key R&D Program of China; contract grant number: 2017YFC0110401
Contract grant sponsor: National Natural Science Foundation of China; contract grant numbers: 51475323, 51520105006, 51721003, 51575377

tensioned. Thanks to the superior foldability, light weight, flexibility, fatigue resistance, and dimensional stability,[28] it is widely used in engineering applications such as medical implants.[29–31] Numerous researches have been conducted to analyze its mechanical properties. Based on the open-coiled spring theory, the geometry and radial/longitudinal stiffness of the braided tube were theoretically analyzed by Jedwab and Clerc,[32] and explicit formulas were proposed to calculate them. With experimental[33] and numerical[34] methods, the radial stiffness was investigated, and the results further validated the theoretical analysis. Besides, investigation of the radial contraction and deformation mode showed the great structural stability of the braid.[35] Additionally, Kim et al.[36] conducted numerical simulations to study the bending behavior of the braided tube, from which the excellent flexibility of the structure was demonstrated.

In this article, we propose a new foldable manipulator with tunable stiffness. The manipulator takes a braided skeleton to enable radial folding, whereas membrane is used to seal the skeleton so as to adjust stiffness through negative pressure. This article is organized as follows. In Section 2, the design of the manipulator is introduced, together with the fabrication process. Next, the bending stiffness of the manipulator is investigated experimentally and numerically in Section 3. Theoretical model and parametric analysis are presented in Section 4. Section 5 presents the discussions. At last, conclusion is given which ends the article.

MANIPULATOR DESIGN AND FABRICATION

Manipulator design

The manipulator is composed of a braided tube as the skeleton and membrane to seal the tube. The geometry of the braided tube is shown in Figure 1A, which is determined by braiding angle β, tube diameter D, tube length L, and the diameter and number of fibers, d and n, respectively.

When longitudinally tensioned/compressed, the tube diameter D changes with β, leading to tube folding/deploying. The fiber can be considered as nearly inextensible during the deformation, and its length l can be calculated by

$$l = \frac{c\pi D}{\cos\beta} = \frac{c\pi D'}{\cos\beta'} \tag{1}$$

where c is the coil number of each fiber which is a constant, and the parameters of the deformed tube are denoted with a prime. Simplifying Eq. (1), the diameter of the deformed tube can be acquired as

$$D' = D\cos\beta'/\cos\beta \tag{2}$$

Theoretically, β ranges between 0° and 90°. D' tends to the upper limit $D/\cos\beta$ when β approaches 0°, and to the lower limit $2d$ when β approaches 90°. As a result, the maximum folding ratio (r), which is the ratio between the maxima and minima of the tube diameter, can be estimated as

$$r = \frac{D}{2d\cos\beta} \tag{3}$$

Since the fibers of the braided tube loosely touch each other at the intersecting points, where the relative movement is only constrained by friction, the braided tube has great bending flexibility and can achieve a large curvature.[36] While the flexibility helps the tube pass tortuous body orifice and achieves an S shape curve during operation, it is not able to provide sufficient support for surgical tools in operation. To achieve tunable stiffness, membrane is adopted to cover both the inner and outer surfaces of the braided tube, forming a tubular sealing cavity. As seen in Figure 1B, the cavity is connected to a pump via an air duct to create vacuum. In the normal flexible state, the braided skeleton of the new manipulator dominates, and the device is flexible and foldable. When the cavity is vacuumed, the device enters the rigid state. In this state, the air pressure compresses the membrane to the braided tube tightly, and the membrane also deforms when bent, thereby improving the stiffness of the manipulator.

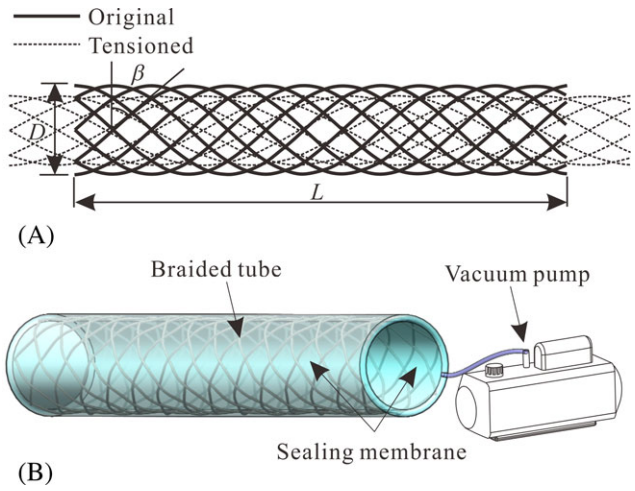

FIGURE 1. The manipulator (A) geometry of the braided tube; (B) overview of the manipulator.

Manipulator fabrication

Nylon fiber was selected to fabricate the braided tube mainly due to its good elasticity and compliance to the 3D printed mold, and low heat treatment temperature. And the polyethylene membrane was used to form the cavity because it was easy to seal and had relatively high tensile stiffness to provide constraining force to the fibers. A simple fabrication procedure was developed as follows. First, a braided tube was constructed,[37] and a tubular polyethylene membrane was fabricated by heat sealing. Second, the tubular membrane was on the braided tube, covering both inner and outer surfaces of the tube. Third, a duct was inserted into the cavity, and the cavity was sealed with glue. A specimen fabricated with the above method together with the vacuum system is shown in Figure 2. Young's modulus of both the nylon fiber and the polyethylene membrane were tested on

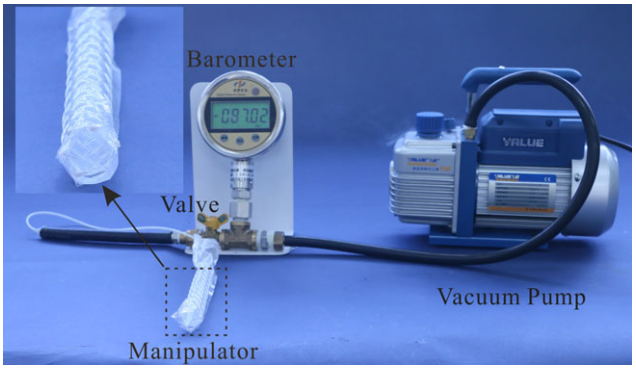

FIGURE 2. Physical specimen of the manipulator and its vacuum system.

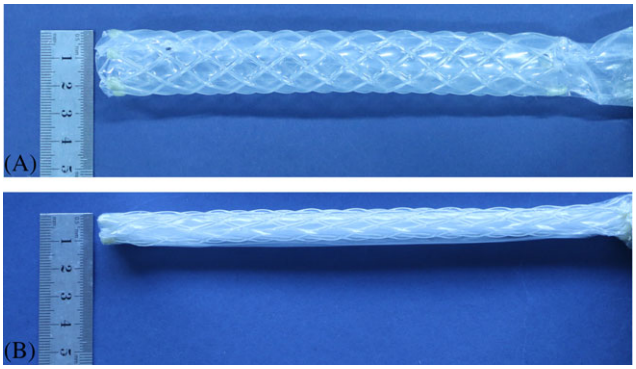

FIGURE 3. (A) Large and (B) small profiles of the manipulator.

an *Instron* 5982 testing machine, and the parameters are listed in Table I.

Moreover, the manipulator can be folded radially by longitudinal tension. It can be seen in Figure 3 that after tension, the diameter of the specimen is reduced from 21.5 mm to 11.0 mm, achieving a radial folding ratio of 1.95. When in place, the initial diameter can be resumed by various approaches. For instance, a balloon, similar to that for medical stents,[38] can be used to expand the manipulator. This feature will greatly facilitate the insertion of the manipulator into a natural orifice.

EXPERIMENTS AND FINITE ELEMENT MODELING

Experimental setup

To evaluate the bending stiffness of the manipulator, pure bending tests were conducted on the physical specimen. The bending tester was designed as Simons and Shockey[39] introduced, and its schema is presented in Figure 4. The transmission wire denoted by the dotted line in the figure is oriented by four fixed pulleys. When the wire is pulled horizontally, a pure moment will be applied to the holder, and transmitted to the tested specimen. The moment can be calculated as

$$M = F\left[\frac{h}{\sin\alpha}\sin(\alpha+\gamma/2) + 2\left(r_p + r_w\right)\right] \quad (4)$$

where r_w and F are radius and force of the transmission wire, respectively; γ is the bending angle, and the other undefined parameters are presented in Figure 4.

TABLE I. Parameters of the Physical Specimen

Parameters	Value
Tube length, L	127.26 mm
Tube diameter, D	19.32 mm
Fiber number, n	12
Fiber diameter, d	1.07 mm
Braiding angle, β	54.43°
Young's modulus of the fibers, E_f	3498.6 Mpa
Young's modulus of the membrane, E_m	291 Mpa
Membrane thickness, b	0.04 mm
Friction coefficient, μ	0.3
Negative pressure, P	67Kpa

The experimental setup is illustrated in Figure 5. The bending tester is put on a flat platform. Two ends of the specimen are fixed on the bending tester. One end of the transmission wire which passes through the bending tester is fixed, and the other is connected to a moveable load cell. Wheels are installed at the corners of the tester for moving on the platform freely. Displacement control is applied in the experiments, and the loading rate is 0.3 mm/s.

Finite element modeling

To understand the behavior of the manipulator in detail, numerical simulations of the bending tests were also conducted using commercial finite element code Abaqus/Explicit.[40] Three parts were established, including the inner and outer membranes and a braided tube, to model the rigid state of the manipulator. For the flexible state, the two membranes were removed and only the braided tube was considered. With the method introduced by Alpyildiz,[41] track of the fibers of the braided tube was determined with the preprocessor Matlab. Information of the nodes and elements of the braided tube were acquired in Matlab, with which an orphan mesh part was established and imported into Abaqus. The nodes at the two ends of the braided tube were, respectively, tied to two reference points, *Rp1* and *Rp2*, as rigid bodies. The geometries of the membranes were established in Abaqus. The diameter of the inner membrane was a little smaller than that of the braided tube, whereas that of the outer membrane was a little larger to avoid physical interference. Beam elements, B31, and membrane elements, M3D4R, were used to mesh the braided tube and the membranes, respectively.

To model the bending process, two analysis steps were defined. First, uniform pressure was applied to the membranes to model the vacuum. Subsequently, the pressure was kept at a constant, while opposite rotations about the

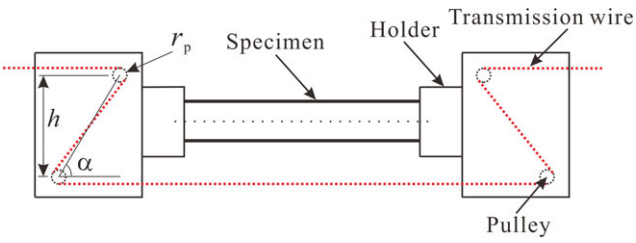

FIGURE 4. Schema of the bending tester.

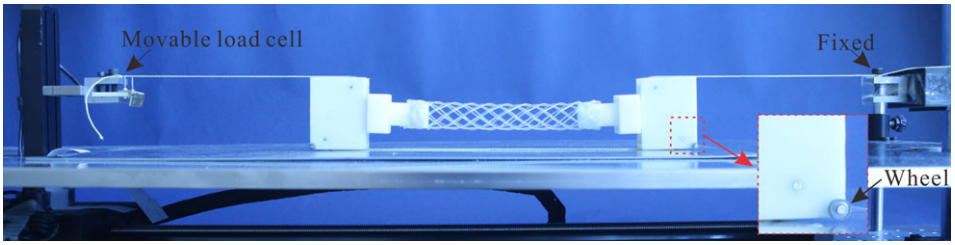

FIGURE 5. Experimental setup.

radius of the manipulator were assigned to the rotational degree of freedoms of the *Rp1* and *Rp2*, respectively, to achieve a 60° bending of the manipulator. Smooth amplitude definition built in Abaqus was utilized to control the bending rate. Friction coefficient was considered and set as 0.3.

Mesh sizes of 0.2 mm for the braided tube, 0.5 mm for the membranes, and step times of 0.005 s and 0.03 s for the two steps, respectively, were determined through convergence tests. The rotation angle and moment of reference point *Rp1* were recorded and output.

RESULTS

Bending of both a manipulator and a stand-alone braided tube were first studied to demonstrate the tunable stiffness. The experiments were, respectively, conducted three times to the tube and the manipulator. Good repeatability was obtained, and the averages of the results were calculated. The experimental and numerical deformed configurations of the manipulator in the rigid state and the stand-alone tube are shown in Figure 6 as representatives. No kinking is observed, indicating the design parameters are appropriate. The experimental moment versus bending angle curves are presented in Figure 7. First compare the experimental curves of the braided tube and the manipulator in the flexible state. A linear response is obtained in both cases, and the two curves almost overlap, with the error between them at a bending angle of 60° being only 4.23%. This result validates the assumption in the numerical simulation that the effect of membrane on bending stiffness in the flexible state is very limited and can be safely ignored. Then the manipulator in the flexible and rigid states are compared. It can be seen that the manipulator shows a highly nonlinear response in the rigid state, and the moment is tremendously raised when negative pressure is applied. At a bending angle of 60°, the bending moment is increased by 585%. To this point, it can be concluded that we have successfully developed a device with two remarkably different states of stiffness.

Numerical simulation results are also presented in Figures 6 and 7 and compared with the experimental results. At a bending angle of 60°, the numerical data of the manipulator and the braided tube are 14.03% and 8.95%, respectively, lower than the experimental ones, see Table II. This error is mainly caused by the frictional consumption existing in the loading tester in Figure 5, which was not considered in the numerical simulation. However, the numerically obtained deformed configurations and moment curves are found to show the same tendency with the respective experimental ones. Therefore the numerical models are deemed reliable to explain the stiffness-enhancing mechanism. In addition, the maximum strain of the membrane and the braided skeleton are 4.9% and 0.06%, respectively, both of which are in the linear elastic stage.

With the validated numerical models, the stiffness-enhancing mechanism of the manipulator in the rigid state is examined in detail. Figure 6C shows the deformed configuration of the braided skeleton of the manipulator in the rigid state. It can be seen that a nearly pure bending with a

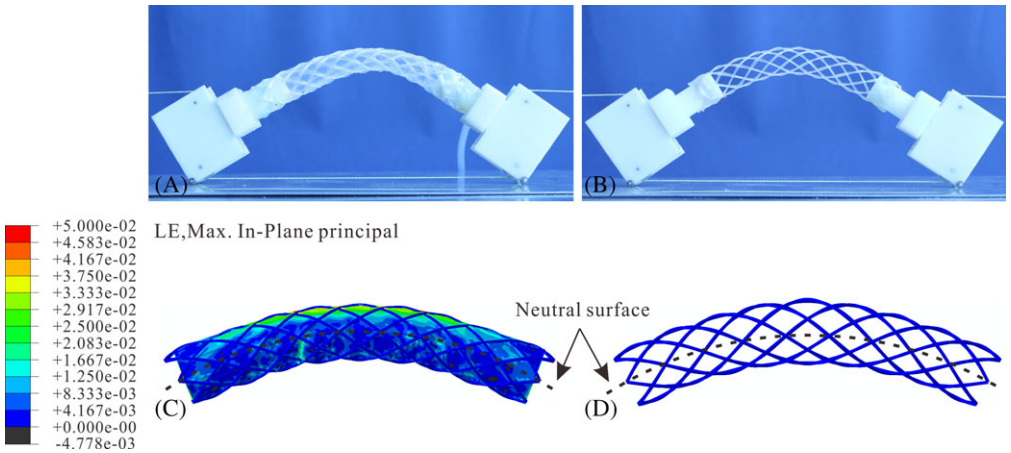

FIGURE 6. Experimental deformed configurations of (A) the manipulator and (B) the stand-alone braided tube, and the numerical ones of (C) the manipulator and (D) the stand-alone braided tube.

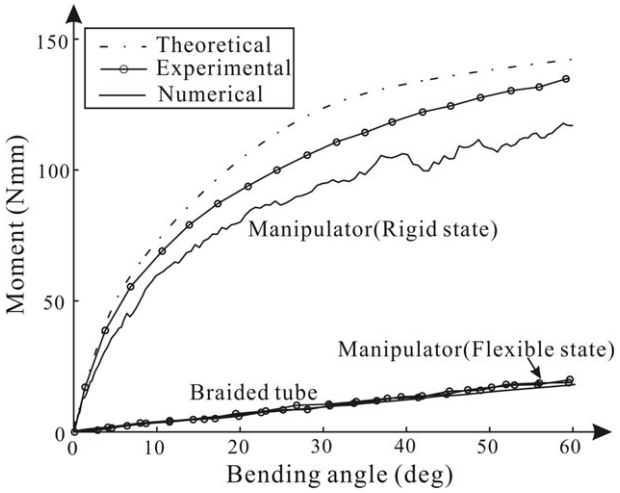

FIGURE 7. Moment versus bending angle curves of both the manipulator and the braided tube.

TABLE II. Moments at a Bending Angle of 60° of Both the Manipulator and the Braided Tube

Specimen	Result	Value (Nmm)	Error
Manipulator, rigid state	Experimental	136.20	—
	Numerical	117.09	14.03%
	Theoretical	142.80	4.85%
Braided tube	Experimental	19.88	—
	Numerical	18.10	8.95%
	Theoretical	17.14	13.78%

measured radius of curvature ρ=136.17 mm, similar to the stand-alone tube in which ρ=144.36 mm in Figure 6D, is obtained. This suggests that in the rigid state where the membrane is tightly compressed on the skeleton, the deformation mode of the manipulator is not significantly affected and can still be treated as pure bending. Then the deformation of the membrane is investigated by drawing the longitudinal (LE11) and circumferential (LE22) strain contours of the outer membrane in Figure 8A,B. It can be seen that the membrane above the neutral surface is longitudinally tensioned, while that below is circumferentially tensioned. This is because the braiding angle above the neutral surface increases after bending, whereas that below decreases as shown in Figure 8A,B, thereby stretching the membrane in different directions. The deformed membrane can sustain load and therefore improve the stiffness of the manipulator. Note that the change in braiding angle also causes circumferential compression above the neutral surface and longitudinal compression below. But since membrane cannot sustain compressive load, the compressive deformation does not contribute to stiffness improvement. In addition, it is observed that the membrane above the neutral surface has a larger strain in the middle than that at the two ends.

THEORETICAL ANALYSIS

Based on the experimental and numerical results, a theoretical model is built in this section to analyze the stiffness of the manipulator in the flexible and rigid states, and to understand the effects of geometric and material design parameters.

Stiffness-enhancing mechanism

In this subsection, the stiffness-enhancing mechanism of the new manipulator is explained in detail through a theoretical analysis of the bending stiffness in the flexible and rigid states.

Flexible state. In the flexible state, the membrane is ignored and the stiffness of the manipulator in this state is assumed to solely depend on the braided tube. According to Wahl[42] and Zhang,[43] the following assumptions can be made on the braided tube: (1) the tube is a combination of a number of independent open-coiled helical springs, (2) the extremities of the tube are not free to rotate, (3) the tube undergoes elastic deformation only, (4) the tube possesses large D/d ratio, (5) the change in braiding angle is ignored. Consequently, the bending stiffness of the braided tube can be determined by

$$EI_{\mathrm{b}} = \frac{2nE_{\mathrm{f}}I_{\mathrm{f}}\sin\beta}{1+\sin^2\beta+\frac{E_{\mathrm{f}}}{2G_{\mathrm{f}}}\cos^2\beta} \tag{5}$$

where I_{f}, E_{f}, and G_{f} are the moment of inertia, Young's modulus, and shear modulus of the fibers, respectively. The relationship between bending moment and bending angle can be expressed as

$$M_{\mathrm{b}} = EI_{\mathrm{b}}\gamma \tag{6}$$

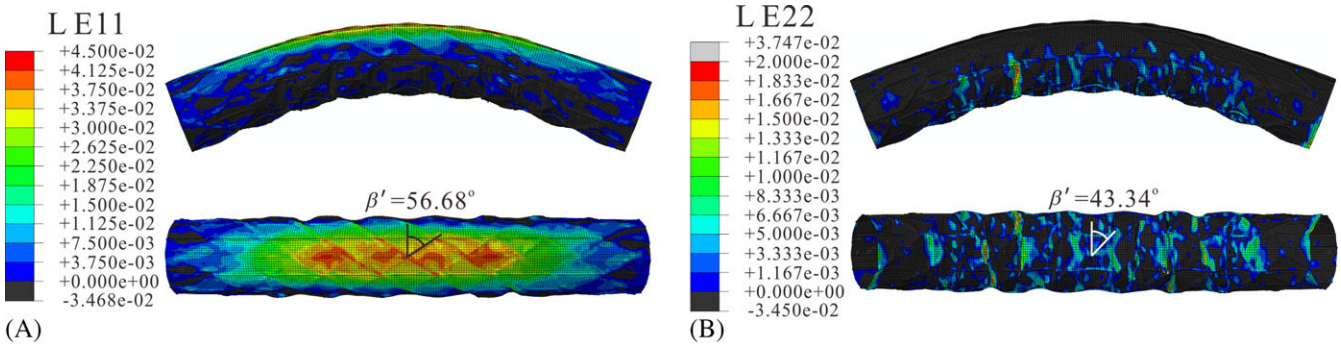

FIGURE 8. (A) Longitudinal and (B) circumferential strain contours of the outer membrane.

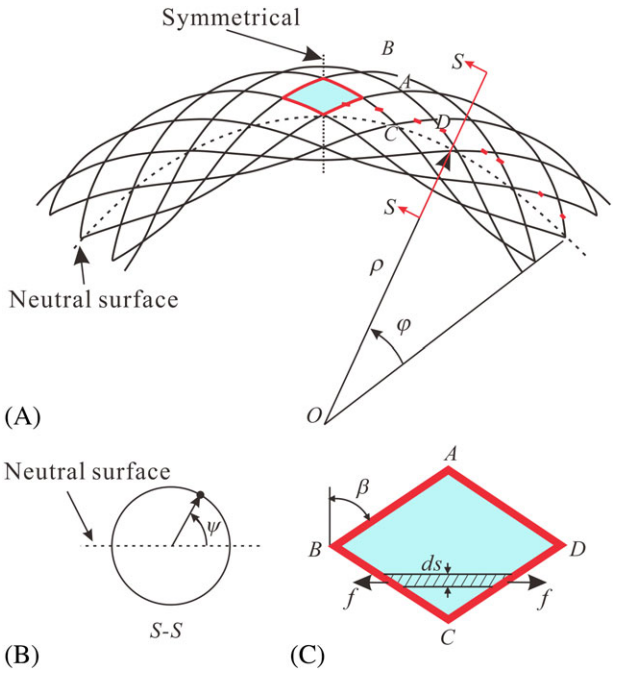

FIGURE 9. Geometry of the bent manipulator: (A) global bending of the manipulator; (B) cross section; (C) a single unit.

Rigid state. In the rigid state, the membrane is compressed by the air pressure onto the braided skeleton tightly, and both components deform simultaneously when bent. The following assumptions are made based on the numerical results: (1) the braided skeleton is also subjected to pure bending (Figure 9A); (2) compression in the membrane is not considered; (3) when the tensile force is small, there is no sliding between the membrane and fibers, and the friction between them provides the tensile force; (4) when the tensile force reaches the maximum static friction, sliding will appear between the membrane and fibers.

According to the assumption of pure bending of the braided skeleton, the longitudinal strain (ε_l) and circumferential strain (ε_c) of the points at the same circular coordinate ψ defined in Figure 9B are identical, which can be, respectively, calculated as

$$\begin{cases} \varepsilon_l = \dfrac{D\gamma \sin\psi}{2L} \\ \varepsilon_c = -\dfrac{D\gamma \sin\psi}{2L}\tan\beta \end{cases} \tag{7}$$

In addition, the elastic strain energy of the braided skeleton can be calculated based on Eq. (5) as $\frac{1}{2}EI_b\gamma^2$.

Regarding the deformation of the membrane, first consider the membrane above the neutral surface ($0^o < \psi < 180^o$) by selecting a unit *ABCD* in Figure 9C. Based on assumption (3), when the tensile force is below the maximum static friction, there is no sliding between the membrane and fibers, and therefore the longitudinal strain of the membrane is identical to that of the braided skeleton. Accordingly, the tensile force of a strip with an infinitesimal circumferential length *ds* at a circular coordinate ψ can be calculated as

$$f = E_m \varepsilon_l b ds \tag{8}$$

Meanwhile, the maximum static friction at the same circumferential length is

$$f_{max} = NP\mu\frac{\pi d}{2\cos\beta}ds \tag{9}$$

where the parameter N is the number of fiber segments highlighted in red, which contributes to the friction, and can be determined by

$$N = \frac{\varphi nL}{\gamma\pi D\tan\beta} \tag{10}$$

When the tensile force rises to the maximum static strain, the membrane strain also reaches its maxima, or the critical strain, which is determined from Eqs. (8–10) as

$$\varepsilon_l' = \frac{\pi\varphi nP\mu d}{\gamma E_m b\sin 2\beta} \tag{11}$$

When the longitudinal strain of the braided skeleton ε_l is smaller than ε_1', the membrane strain is equal to ε_l. When it exceeds ε_l', according to assumption (4), the membrane slides along the braided skeleton and its longitudinal strain stays constant at ε_l'. In this case, the energy is contributed by two parts: the elastic strain energy of the membrane, and the work done by the sliding friction force, which is considered as identical to the maximum static friction force. As a result, the energy density above the neutral surface can be calculated as

$$W(\varepsilon_l) = \begin{cases} \dfrac{1}{2}E_m b\varepsilon_l^2 & (\varepsilon_l \le \varepsilon_l') \\ E_m b\varepsilon_l'(\varepsilon_l - \varepsilon_l'/2) & (\varepsilon_l > \varepsilon_l') \end{cases} \tag{12}$$

For the membrane below the neutral surface ($180^o < \psi < 360^o$), only the circumferential tensile deformation is considered. The same approach is used and both the critical strainε_c' and the energy density$W(\varepsilon_c)$ can be determined.

With the analysis above, the total energy of the manipulator in the rigid state can be obtained by summing up the energies contributed by the braided skeleton, the membrane, and the sliding friction if it exists

$$E_t = 2\frac{LD}{\gamma}\left[\int_0^{\pi\gamma/2}\int_0 W(\varepsilon_l)d\varphi d\psi + \int_{\pi}^{2\pi\gamma/2}\int_0 W(\varepsilon_c)d\varphi d\psi\right] + \frac{1}{2}EI_b\gamma^2 \tag{13}$$

Applying balance between internal energy and external work, the bending moment can be determined as

$$M_s = dE_t/d\gamma \tag{14}$$

The bending moment of the manipulator with parameters listed in Table I is calculated with Eq. (14) and vaidated with the expeirmental result in Figure 7. The theoretical and

TABLE III. Design Parameters of the Theoretical Models

Group	E_m(Mpa)	P(Kpa)	E_m(Gpa)	n	β (°)	d(mm)
1	50~300	30	3.5	12	54.43	1.07
2	50~300	50	3.5	12	54.43	1.07
3	50~300	67	3.5	12	54.43	1.07
4	100	0~100	3.5	12	54.43	1.07
5	200	0~100	3.5	12	54.43	1.07
6	400	0~100	3.5	12	54.43	1.07
7	100	67	0.5~9.5	12	54.43	1.07
8	100	67	3.5	12~36	54.43	1.07
9	100	67	3.5	12	30~60	1.07
10	100	67	3.5	12	54.43	0.5~1.2

experimental curves show the same trend, and the differnece between them at a bending angle of 60° is only 4.85%, indicating the accurary of the theoretical model.

Effects of the design parameters

With the theoretical model, the effects of design parameters on the stiffness of the manipulator are analyzed here. The design parameters are classified into three categories: membrane parameters E_m and b, membrane-skeleton interaction parameters P and μ, and braided-skeleton parameters E_f, n, β, and d. The design parameters of the theoretical models are listed in Table III, and the other parameters are the same as those of the physical specimen listed in Table I.

Effects of the membrane parameters. According to Eqs. (11) and (12), the thickness b and Young's modulus E_m of the membrane affect the stiffness of the manipulator in the same manner through the term $E_m b$, which can be considered as membrane stiffness. To investigate the effects of membrane stiffness, b is set to be 0.04 mm, and E_m varies from 50 Mpa to 300 Mpa. The moments at a bending angle of 30°, denoted by M_{30}, are calcauted from Eq. (14), and the relationships between M_{30} and E_m at different negative pressures P are drawn in Figure 10A. The results of the manipulator in the flexible state are also presented as a benchmark. Two observations can be made from the curves. First, M_{30} increases with E_m, indicating that a stronger membrane leads to a higher bending moment. The reason is that the tensile force carried by the membrane increases with the membrane stiffness. Second, the slopes of the curves, on the other hand, reduce with E_m. This suggests that increasing E_m is more effective when it is relatively small. Therefore in practice, the membrane need not to be too stiff. According to Figure 10A, a membrane with $E_m = 5 \times 10^3 P$ is stiff enough for a membrane with thickness b of 0.04 mm.

Effects of membrane-skeleton interaction. Similarly, the negative pressure P and friction coefficient μ theoretically play the same role in the stiffness of the manipulator for the friction is proportionable to $P\mu$ according to Eq. (11). Here we set μ as 0.3 and vary P from 0 Kpa to 101 Kpa to analyze the effect of friction. M_{30} at different P and E_m are theoretically calculated from Eq. (14), and the results are presented in Figure 10B. Generally M_{30} increases sharply with P, especially when E_m is large. This result clearly demonstrates that applying negative pressure is effective at tuning the bending stiffness of the manipulator.

Effects of the braided-skeleton parameters. The effect of the Young's modulus of the fibers E_f is firstly invetigated by varying it from 0.5 Gpa to 9.5 Gpa. As shown in Figure 11A, a linear response is obtained in both the rigid and flexible states. This is understandable as E_f only linearly increases the bending moment taken by the braided skeleton, which is clearly seen in Eqs. (6) and (13).

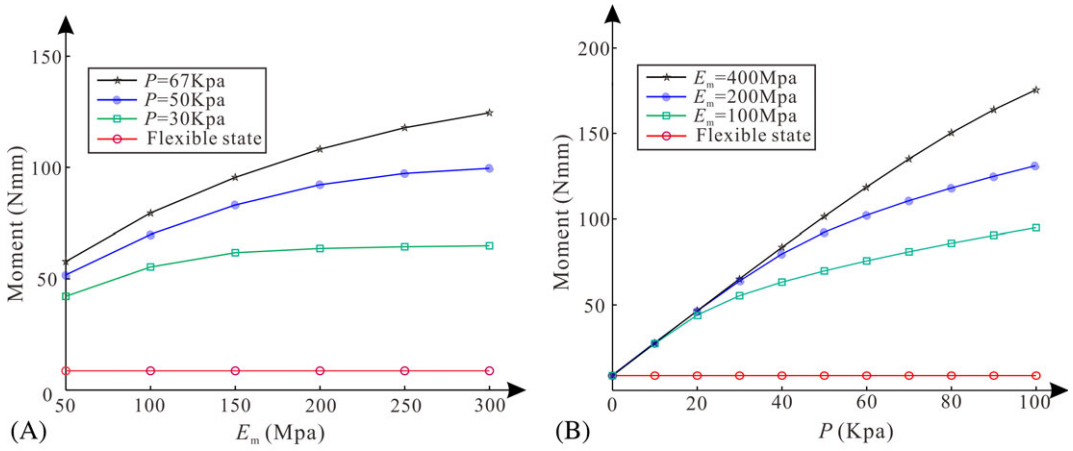

FIGURE 10. Effects of membrane stiffness and friction: (A) M_{30} versus E_m curves at different P; (B) M_{30} versus P curves at different E_m.

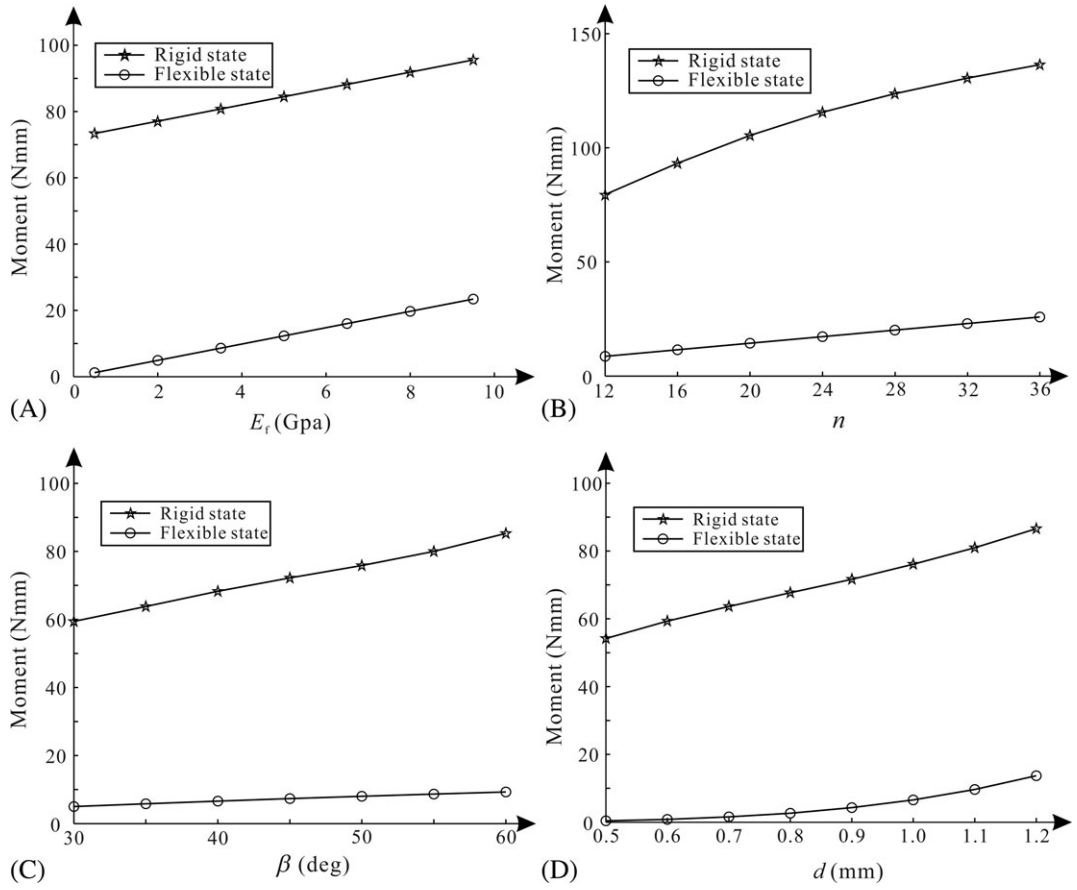

FIGURE 11. Effects of the properties of the braided skeleton: relationships between M_{30} and (A) E_f, (B) n, (C) β, (D) d.

The other three parameters, while mainly affecting the bending stiffness of the braided skeleton as in the case of EI_b, also slightly change the friction due to variation in the number and size of the quadrilateral units in the braided skeleton. The effects of the three paramters on the bending moments are, respectively, drawn in Figure 11B-D. It can be seen that all the parameters leads to increase in bending stiffness in both states. And roughly linear relationships are invariably obtained.

DISCUSSIONS

In engineering applications, determination of the manipulator design parameters is always multiobjective. Besides the stiffness in the rigid state, factors such as size, flexibility, and folding ratio, also need to be taken into consideration. Those factors are mainly controlled by the properties of the braided skeleton. As a result, practically it is beneficial to tune the stiffness of the manipulator in the rigid state through adjusting the membrane and the membrane-fiber friction. As discussed in the previous sections, a large stiffness can be achieved by increasing the Young's modulus and thickness of the membrane, the negative pressure, and the friction coefficient.

It has been mentioned that stiffness and size are two key parameters to evaluate the performance of a manipulator. Regarding stiffness, it has been found out that the size and testing method varied greatly among different designs, making direct comparison of the stiffness among them very difficult. As a result, endoscopes which have a similar operation procedure and readily available bending stiffness data are adopted as benchmarks to evaluate the stiffness of the new device.[24] Currently, commercial endoscopes have a bending stiffness ranging from 160 to 240 Ncm^2.[44] A manipulator with bending stiffness lower than 160 Ncm^2 in the flexible state and much larger than 240 Ncm^2 in the rigid state is considered to be able to satisfy both easy access and adequate support for surgical tools. Toward this objective, we designed a manipulator with the design parameters listed in Table IV. Since the new manipulator has a nonlinear relationship between moment versus bending angle, the bending stiffness is calculated as the tangent stiffness at a bending angle of 30°, that is,

$$EI = M_{30}L/(\pi/6) \tag{15}$$

Based on the previously developed theoretical model, the bending stiffness is 63.92 Ncm^2 in the flexible state, only 40% of the softest commercial endoscope. In the rigid state, it reaches 515.96 Ncm^2, 115% higher than that of the stiffest commercial endoscope, which is deemed suitable for MIS.

TABLE IV. Design Parameters of the Manipulator for MIS

Parameters	Value
Tube length, L	100 mm
Tube diameter, D	20 mm
Fiber number, n	18
Fiber diameter, d	1 mm
Braiding angle, β	50°
Young's modulus of fibers, E_f	10000 Mpa
Young's modulus of membrane, E_m	500 Mpa
Membrane thickness, b	0.04 mm
Friction coefficient, μ	0.3
Negative pressure, P	101 Kpa

Regarding size, the braided manipulator is advantageous for its large folding ratio. In addition, the braided manipulator can achieve a relatively small wall thickness while providing sufficient stiffness. For instance, the wall thickness of the design in Table IV is about 2 mm, lower than that of many existing devices ranging from 3.5 to 4 mm.[17,25,45] This is also desirable as it enables larger lumen for surgical tools and other devices.

CONCLUSIONS

In this article, we propose a novel manipulator for minimal invasive surgery. The device is composed of a braided tube skeleton to achieve longitudinal flexibility and radial folding, and membrane which seals the tube to obtain tunable stiffness through negative pressure. Experimental and numerical results indicate in the flexible state, the braided tube and the membrane are loosely contacted, and the bending stiffness is predominantly provided by the braided skeleton. In the rigid state the membrane is compressed on the braided tube by creating a vacuum inside, whereas the membrane is tensioned by the braided tube, leading to an increase in bending stiffness by 585%. Meanwhile, the device achieves a radial folding ratio of 1.95, making it much easier to pass it through tortuous natural orifices. Based on the experimental and numerical results, a theoretical model has been developed to calculate the bending stiffness in the rigid state, which agrees reasonably well with experiments. Furthermore, a systematic parametric study has been conducted to investigate the effects of design parameters. It has been found out that the Young's modulus and thickness of the membrane, which indicate membrane stiffness, and the negative pressure and friction coefficient between the tube and the membrane, which indicate the friction force, are effective at improving the stiffness in the rigid state. The stiffness in the flexible state, on the other hand, is mainly determined by the design parameters of the braided tube. By tuning the parameters, we have successfully designed a manipulator which has a bending stiffness in the rigid state more than twice as large as that for commercial endoscopes, and in the flexible state less than half. This makes the new device ideal for MIS applications.

Despite the promising results, the work still has limitations because it has not provided a prototype, which has a control system and is integrated with surgical tools. For future research, a control system for accurate positioning of the manipulator when in operation will be developed. And the manipulator will be integrated with surgical tools to test its performance through in vitro and in vivo experiments.

ACKNOWLEDGMENTS

This work was supported by the National Natural Science Foundation of China (Grant 51475323), the National Key R&D Program of China (Grant No. 2017YFC0110401) and the National Natural Science Foundation of China (Grant 51575377, Grant 51721003 and Grant 51520105006).

REFERENCES

1. Tsui C, Klein R, Garabrant M. Minimally invasive surgery: National trends in adoption and future directions for hospital strategy. Surg Endosc 2013;27:2253–2257.
2. Choi H, Kwak HS, Lim YA, Kim HJ. Surgical robot for single-incision laparoscopic surgery. IEEE T Bio-Med Eng 2014;61:2458–2466.
3. Liska D, Lee SW, Nandakumar G. Laparoscopic surgery for benign and malignant colorectal diseases. Surg Laparo Endo Per 2012;22: 165–174.
4. Goldman RE, Bajo A, Maclachlan LS, Pickens R, Herrell SD, Simaan N. Design and performance evaluation of a minimally invasive telerobotic platform for transurethral surveillance and intervention. IEEE T Bio-Med Eng 2013;60:918–925.
5. Stiff G, Rhodes M, Kelly A, Telford K, Armstrong CP, Rees BI. Long-term pain: Less common after laparoscopic than open cholecystectomy. Br J Surg 1994;81:1368–1370.
6. Tacchino R, Greco F, Matera D. Single-incision laparoscopic cholecystectomy: Surgery without a visible scar. Surg Endosc 2009;23: 896–899.
7. Zornig C, Mofid H, Emmermann A, Alm M, von WHA, Felixmuller C. Scarless cholecystectomy with combined transvaginal and transumbilical approach in a series of 20 patients. Surg Endosc 2008;22: 1427–1429.
8. Keus F, Jong JD. Laparoscopic versus open cholecystectomy for patients with symptomatic cholecystolithiasis *Cochrane*. Db Syst Rev 2006;18:CD006231.
9. Richards WO, Rattner DW. Endoluminal and transluminal surgery: No longer if, but when. Surg Endosc 2005;19:461–463.
10. Moris DN, Bramis KJ, Mantonakis EI, Papalampros EL, Petrou AS, Papalampros AE. Surgery via natural orifices in human beings: Yesterday, today, tomorrow. Am J Surg 2012;204:93–102.
11. National Orifice Surgery Consortium for Assessment and Research (NOSCARTM). 2006. Working Group Summary on Development of A Multitasking platform. Available from: http://www.noscar.org/presentations-2006/tasking-platform. Access October 2006.
12. Rattner D, Kalloo A. ASGE/SAGES working group on natural orifice translumenal endoscopic surgery. Surg Endosc 2006;63:199–203.
13. Thompson CC, Ryou M, Soper NJ, Hungess ES, Rothstein RI, Swanstrom LL. Evaluation of a manually driven, multitasking platform for complex endoluminal and natural orifice transluminal endoscopic surgery applications (with video). Gastrointest Endosc 2009;70:121–125.
14. Ponsky JL. Endoluminal surgery: Past, present and future. Surg Endosc 2006;20:S500–S502.
15. Zuo S, Wang S. Current and emerging robotic assisted intervention for NOTES *Expert*. Rev Med Devic 2016;13:1095–1105.
16. Shaikh SN, Thompson CC. Natural orifice translumenal surgery: Flexible platform review. World J Gastrointest Surg 2010;2: 210–216.
17. Zhao R, Yao Y, Luo Y. Development of a variable stiffness over tube based on low-melting-point-alloy for endoscopic surgery. J Med Devices 2016;10:303–310.
18. Li J, Li X, Wang J Xing Y, Wang S, Ren X. Design and evaluation of a variable stiffness manual operating platform for laparoendoscopic single site surgery (LESS). Int J Med Robot Comp 2017;13:e1797.
19. Cheng N, Ishigami G, Hawthorne S, Chen H, Hansen M, Telleria M, Playter R and Iagnemma K 2010 Design and analysis of a soft

mobile robot composed of multiple thermally activated joints driven by a single actuator. Proc Robotics and Automation (ICRA), Piscataway, NJ: IEEE 5207-5212
20. Loeve AJ, Bosma JH, Breedveld P, Dodou D, Dankelman J. Polymer rigidity control for endoscopic shaft-guide 'Plastolock'- a feasibility study. J Med Devices 2010;4:045001.
21. Dong H, Walker GM. Adjustable stiffness tubes via thermal modulation of a low melting point polymer. Smart Mater Struct 2012;21:317–321.
22. Kim YJ, Cheng S, Kim S, Iagnemma K. A novel layer jamming mechanism with tunable stiffness capability for minimally invasive surgery. IEEE T Robot 2013;29:1031–1042.
23. Loeve AJ, Plettenburg DH, Breedveld P, Dankelman J. Endoscope shaft-rigidity control mechanism: "FORGUIDE". IEEE T Bio-Med Eng 2012;59:542–551.
24. Zuo S, Iijima K, Tokumiya T, Ken M. Variable stiffness outer sheath with "dragon skin" structure and negative pneumatic shape-locking mechanism. Int J Comput Ass Rad 2014;9:857–865.
25. Yagi A, Matsumiya K, Masamune K, Liao H and Dohi T 2006 Rigid-flexible outer sheath model using slider linkage locking mechanism and air pressure for endoscopic surgery. International Conference on Medical Image Computing and Computer-Assisted Intervention (MICCAI), 503-510
26. Pellegrino S. Deployable Structures. Vienna, Austria: Springer; 2001.
27. De BM, Van CS, Mortier P, Loo DV, Impe RV, Verdonck P. Virtual optimization of self-expandable braided wire stents. Med Eng Phys 2009;31:448–453.
28. Hu J. 3-D Fibrous Assemblies: Properties, Applications and Modelling of Three-Dimensional Textile Structures. CRC Press; 2008.
29. Bouillot P, Brina O, Ouared R, Yilmaz H, Farhat M, Erceg G. Geometrical deployment for braided stent. Med Image Anal 2016;30:85–94.
30. Yuksekkaya ME, Adanur S. Analysis of polymeric braided tubular structures intended for medical applications. Text Res J 2009;79:99–109.
31. Maetani I, Shigoka H, Omuta S, Gon K, Saito M. What is the preferred shape for an esophageal stent flange? Digest Endosc 2012;24:401–406.
32. Jedwab MR, Clerc CO. A study of the geometrical and mechanical properties of a self-expanding metallic stent--theory and experiment. J Appl Biom 1993;4:77–85.
33. Wang R, Ravichandar K. Mechanical response of a metallic aortic stent—Part I: Pressure-diameter relationship. J Appl Mech-T ASME 2004;71:697–705.
34. Ni XY, Pan CW, Prusty BG. Numerical investigations of the mechanical properties of a braided non-vascular stent design using finite element method. Comput Method Biomec 2015;18:1117–1125.
35. Ochola J, Malengier B, Daelemans L, Langenhove LV. Finite element simulations to evaluate deformation of polyester tubular braided structures. Text Res J 2017;87:1275–1283.
36. Kim JH, Kang TJ, Yu WR. Mechanical modeling of self-expandable stent fabricated using braiding technology. J Biomech 2008;41: 3202–3212.
37. Shang Z, Wang S, You Z, Ma J. A hybrid tubular braid with improved longitudinal stiffness for medical catheter. J Mech Med Biol 2018;1950003. https://doi.org/10.1142/S0219519419500039.
38. Duerig TW, Wholey M. A comparison of balloon- and self-expanding stents. Min Invas Ther Allied Technol 2002;11:173–178.
39. Simons J W and Shockey D A 2006 Mechanical testing devices for characterizing stents *SMST* Conference
40. Abaqus Analysisi User's Manaul, Abaqus documentation version 6.14-1, 2014, dassault sys- tems SIMULA Corp. Providence, RI.
41. Alpyildiz T. 3D geometrical modelling of tubular braids. Text Res J 2012;82:443–453.
42. Wahl AM. Mechanical Spring. New York: McGraw-Hill; 1963.
43. Zhang Y. Spring. Beijing, China: China Machine; 1982 (in Chinese).
44. Hellier D, Albermani F, Evans B, de VH, Adam C, Passenger J. Flexural and torsional rigidity of colonoscopes at room and body temperatures. P I Mech Eng H 2011;225:389–399.
45. Kim YJ, Cheng S, Kim S, Karl I. A stiffness-adjustable hyperredundant manipulator using a variable neutral-line mechanism for minimally invasive surgery. IEEE T Robot 2014;30:382–395.